Mathematical Biology and Bioinformatics
2015. V. 10. № 2. P. 436–454. doi: 10.17537/2015.10.436

========== **MATHEMATICAL MODELING** ==========

УДК: 577.35

Functional heterogeneity arising due to electrical and mechanical interactions between cardial myocytes in mathematical model of homogeneous myocardial fiber

Kursanov A.G.[*1,2], Katsnelson L.B.[1,2], Vikulova N.A.[1,2], Solovyova O.E.[1,2], Markhasin V.S.[1,2]

[1]*Institute of Immunology and Physiology, Ural Branch of the Russian Academy of Sciences, Ekaterinburg, Russia*
[2]*Ural Federal University, Ekaterinburg, Russia*

Abstract. We developed a mathematical model describing heart muscle strand as a one-dimensional continuous medium of cardiomyocytes, through which electrical excitation propagates and excites the cells for contraction. Intracellular excitation-contraction coupling is presented by means of our earlier published model describing mechanical function of the cardiomyocyte evoked by action potential development and calcium activation of cross-bridge formation. The whole strand model simulates also mechanical interaction between the cardiomyocytes in the tissue and accounts for both intracellular and intercellular electro-mechanical coupling and mechano-electric feedback mechanisms. Numerical experiments with the strand formed of initially identical cardiomyocytes revealed that electrical and mechanical interaction between the cells, as well as intracellular mechano-electric feedbacks caused pronounced nonuniformity of their behavior. Model analysis suggests that cooperative mechanisms of myofilament calcium activation play the key role in dynamic adjustment of electrical and mechanical activity of the interacting cardiomyocytes in the tissue.

Key words: *myocardium contraction, cardiomyocyte interaction, excitation-contraction coupling, cardiac mechano-electric feedback, cooperativity.*

INTRODUCTION

Mathematical modeling is an advanced tool for describing cardiac performance that helps to analyze myocardium functions at various levels of the heart organization: from molecules and cells to the whole organ [4, 13, 25]. We have earlier created mathematical models to study the effects of electrical and mechanical interactions between myocardial tissue segments [23] including a muscle duplex approach and discrete chain models, where two or several cardiac muscle segments connected in-series or in-parallel interact mechanically with each other [23, 24]. In the framework of these discrete models we showed that the time lag in electrical excitation of the segments actually intrinsic to the activation of various region of the heart wall resulted in gradual changes in their behavior producing functional heterogeneity of the myocardium system [17].

The most significant limitation of the above mathematical models was that the excitation sequence in these models was prescribed with help of the time delays of the regional stimulation, while electrotonic interactions between cardiomyocytes were not accounted for. In other words, there was quite simplified description of excitation propagation through the tissue.

[*]alexander.kursanov@gmail.com

Our new continuous one-dimensional (1D) mathematical model of the heart muscle strand formed of mechanically and electrically interacting cardiomyocytes connected in-series allowed us to lift the above restrictions.

For the first time this continuum model was described in our recent brief article [10], but there we have published almost exclusively equation of the model and only skimmed over the examples of its use. Unlike that publication, here the model is applied substantially to analyze electromechanical activity of the myocardial tissue. Specifically, to focus mainly on the effects of cardiac MEF in the model, we started with the muscle strand consisting of cardiomyocytes with identical electrical and mechanical properties.

Both micro- and macrocircuits of the electro-mechanical and mechano-electric coupling in cardiac tissue are taken into account in the model (Fig. 1). At the cellular level, electro-mechanical coupling (ECC) and mechano-electric feedback (MEF) between the membrane action potential (AP) generation and cellular contraction are provided by the mechano-dependence of intracellular calcium kinetics [24]. Mechanisms of cooperativity in the kinetics of regulatory calcium-troponin complexes and force-generating acto-myosin cross-bridges underlie this mechano-dependence. At the tissue level, electrical waves of depolarization and repolarization and mechanical wave of deformation arising due to the electrical and mechanical coupling between cardiomyocytes also affect each other. ECC and MEF mechanisms in the heart on the cellular level have been widely discussed [15], but the influence of the mechanical interactions between cells on properties of the electrical wave in myocardium remains largely unappreciated.

To focus mainly on the effects of cardiac MEF in the model, we started with the muscle strand consisting of cardiomyocytes with identical electrical and mechanical properties. In this case only initial asynchrony of the cardiomyocyte activation induced by the excitation wave propagation gives rise to the complicated pattern of the electrical and mechanical interactions between the cells of the strand. This is a similar approach to what we used earlier to study effects of cardiac heterogeneity in muscle duplexes and chains of in-series muscle segments [23, 24]. It was shown that even in the inherently homogeneous cardiac system, the time delays in activation and mechanical interactions between identical muscle segments result in a negative inotropic response and produce gradients of the electro-mechanical characteristics of cardiomyocytes in interacting elements (action potential duration (*APD*), duration of Ca^{2+} transient, sarcoplasmic reticulum Ca^{2+} load, etc [23, 24]). Here, we revise these results by utilizing a more adequate model of cardiac tissue.

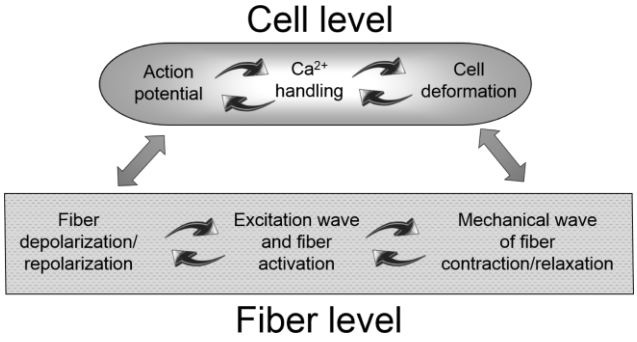

Fig. 1. Scheme of electro-mechanical coupling in the myocardium at the cellular level and tissue level.

We demonstrate model simulations of heart muscle contractions in different mechanical modes: (1) isometric contractions and (2) isotonic contractions under different mechanical loads. The study of these contraction modes is important for understanding the mechanisms regulating different phases of ventricular contraction in the intact heart. The isometric mode of myofiber contraction is consistent with the isovolumeric phase, while the isotonic mode simulates myocardial activity during the ejection phase of ventricle contraction. We also

discuss the effects of slowing down excitation wave propagation on the electro-mechanical performance of cardiac fiber to analyze possible consequences of such an arrhythmogenic factor.

MATHEMATICAL MODEL

We assume a heart muscle fiber as a 1D strand formed of coupled cardiomyocytes. Excitation wave is originated at one edge of the strand and spreads through the cardiomyocytes along the fiber, activating its contraction. It should be emphasized that real fibers in the ventricle walls undoubtedly are branching multiplex structures rather than one-dimensional ones. Nevertheless, simplified consideration of 1D myocardial "fibers" specifying main directions of both the electrical wave spread and mechanical in-series interactions seems to be appropriate to analyze excitation-contraction coupling and mechano-electric feedbacks in myocardial tissue.

As the size of the cardiomyocytes is sufficiently small compared to the characteristic dimensions of myocardial fibers, any cardiomyocyte of the fiber can be considered as an isopotential point of myocardial tissue [22]. In this case, the fiber may be considered as a continuous 1D medium. On the other hand, each cardiomyocyte of the fiber has its own local, dynamically changing geometry and continuously changes its position in macrospace during the contractile cycle of the fiber. On the macrolevel, local deformations originate the dynamic change in each point (cell) position within the fiber geometry. Thus, an electrical wave of excitation propagates along such a dynamically deformable medium. Therefore, two geometrical spaces are considered in the model:

1. microspace representing cellular geometry;
2. macrospace representing the fiber geometry.

In addition, a relationship between these spaces should be defined in the model to determine the mechanical activity of both the fiber and its cells.

Let us consider a 1D muscle strand of a fiber with slack length L and with a single spatial coordinate x varying along the fiber (Fig. 2).

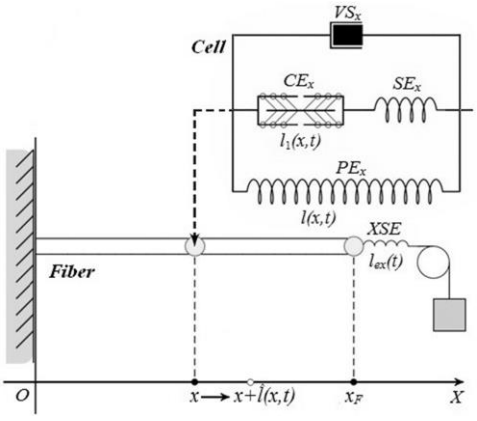

Fig. 2. Scheme of a 1D heart muscle strand. The rheological scheme shows a model of a single cardiomyocyte of coordinate x, where a contractile element (CE_x) is connected to in-series and parallel passive elastic elements (SE_x, PE_x), and a viscous element (VS_x) is in-parallel to PE_x. *XSE* is an external in-series elastic element. Variables $l(x, t)$, $l_1(x, t)$, $l_{ex}(t)$ define deformations of PE_x, CE_x, and *XSE*, respectively, relative to their slack lengths.

The left boundary of the strand is assigned with the origin $x = 0$, the right boundary has a coordinate $x_F = L$ (Fig. 2). We assume that the unstretched fiber consists of unstretched cardiomyocytes of identical lengths with a corresponding sarcomere slack length of 1.67 μm. Thus, each point of the medium is identified by a coordinate $x\{x \mid x \in [0, x_F]\}$, meaning the distance from the left end of the fiber to this point when the fiber is unstretched and

unexcited. The Lagrangian point coordinate does not depend on possible displacements of the material point along the axis during the contractile cycle of the fiber. In other words, if the material point is labeled as x at the slack length state of the fiber, this label will further identify this point (cell) during any fiber deformations.

Electrical and mechanical activity of cells is described by the Ekaterinburg-Oxford mathematical model (EO model) of a single cardiomyocyte [8, 24] (see http://models.cellml.org/e/b9/ for the full set of equations and parameters).

Mechanics of the cellular level (microlevel)

Figure 2 shows a rheological scheme of a single cardiomyocyte at point x (further, cell x). Active contractile element CE_x is associated with the cardiomyocyte sarcomeres. Sarcomeres generate mechanical force in cell x and cell shortening during isotonic contractions due to interactions between actin and myosin and cross-bridges formation. This occurs along with calcium binding to the regulatory protein troponin C (CaTnC complexes). Detailed interactions between these molecular processes are described in our previous papers [5,9].

Suppose $l_1(x, t)$ is the relative change in the length of CE_x of cells x against its slack length (normalized by the sarcomere slack length of 1.67 μm). The force generated by CE_x is defined in the model as

$$F_{CE_x} = F_{CE}(x,t) = \lambda(x) \cdot N(x,t) \cdot p(x, \dot{l}_1(x,t)), \quad (1)$$

where $p(x, \dot{l}_1(x,t))$ is an explicit function that specifies the average force developed by a cross-bridge depending on $\dot{l}_1(x,t)$, which is the velocity of CE_x shortening/stretching; $N(x, t)$ is the concentration of force-generating cross-bridges in CE_x; $\lambda(x)$ is a scale coefficient.

Further, we often skip coordinate x for intracellular variables and coefficients, keeping in mind that each cell x in the fiber may have its own set of coefficient values.

Fraction of cross-bridges $N(x, t)$ in cell x at moment t results from the kinetics of cross-bridges attachment/detachment. $N(x, t)$ not only directly affects mechanical behavior of the contractile element but is a function of it as well:

$$\frac{dN}{dt} = k_+([\mathrm{Ca}_{\mathrm{TnC}}], l_1, \dot{l}_1) \cdot (1 - N) - k_-(\dot{l}_1) \cdot N, \quad (2)$$

where $k_+([\mathrm{Ca}_{\mathrm{TnC}}], l_1, \dot{l}_1)$ and $k_-(\dot{l}_1)$ are the on- and off-rate "constants", respectively, of force-generating cross-bridges cycling. This kinetics depends non-linearly on the concentration of CaTnC complexes ($[\mathrm{Ca}_{\mathrm{TnC}}](t)$) and on both the length of CE_x and on the velocity of its deformation (i.e., on the variables $l_1(t)$ and $\dot{l}_1(t)$).

The kinetics of $[\mathrm{Ca}_{\mathrm{TnC}}]$ is described by the equation

$$\frac{d[\mathrm{Ca}_{\mathrm{TnC}}]}{dt} = k_{on} \cdot ([\mathrm{Ca}_{\mathrm{TnC}}]_{tot} - [\mathrm{Ca}_{\mathrm{TnC}}]) \cdot [\mathrm{Ca}^{2+}]_i - k_{off}(N, [\mathrm{Ca}_{\mathrm{TnC}}]) \cdot [\mathrm{Ca}_{\mathrm{TnC}}], \quad (3)$$

where $[\mathrm{Ca}^{2+}]_i(t)$ is the intracellular free Ca^{2+} concentration; k_{on} is the rate constant of CaTnC association, $k_{off}(N,[\mathrm{Ca}_{\mathrm{TnC}}])$ is the rate "constant" of CaTnC dissociation, which is a function of the mechanical state of the contractile element (variable $N(t)$) and calcium kinetics ($[\mathrm{Ca}_{\mathrm{TnC}}](t)$).

This highly non-linear functional dependence of k_{off} on the current state of sarcomere activity reflects mechanisms of cooperative calcium activation of the contractile proteins: affinity of troponin C for Ca^{2+} increases k_{off} decreases with an increase in (a) the fraction of force-generating cross-bridges $N(t)$ and (b) $[\mathrm{Ca}_{\mathrm{TnC}}](t)$. Mechano-dependent cross-bridges kinetics affect the CaTnC kinetics and thereby the Ca^{2+} kinetics, i.e., both become mechano-

sensitive. Cooperative mechanisms of CaTnC kinetics as well as respective equations are identified and justified in our previous papers [5, 8, 24].

Thus, direct links and feedback between Ca^{2+} kinetics, CE_x deformations, and force generation are defined in the EO model and ensured from the cooperative mechanisms of myofilament Ca^{2+} activation.

Besides the active contractile element CE_x, in the rheological scheme of cardiomyocyte x there are also elastic and viscous elements (SE_x, PE_x, and VS_x, Fig. 2), which mainly determine mechanical properties of passive myocardium but also may modulate the active myocardial mechanics [8].

Suppose $l(x, t)$ is a relative cell x length change per sarcomere (normalized by its sarcomere slack length). In correspondence with the rheological scheme, $l(x, t)$ coincides with the deviation of the length of the parallel elastic element PE_x from its slack length.

Forces generated by SEx and PE_x are defined as follows:

$$F_{SE_x} = F_{SE}(x,t) = \beta_1 \cdot (e^{\alpha_1 \cdot (l(x,t) - l_1(x,t))} - 1), \quad (4)$$

$$F_{PE_x} = F_{PE}(x,t) = \beta_2 \cdot (e^{\alpha_2 \cdot l(x,t)} - 1), \quad (5)$$

with parameters α_1, β_1, α_2 and β_2 justified in our previous works.

The viscosity coefficient of the damper VS_x in the rheological scheme of the cardiomyocyte is considered to be dependent on the degree of stretching the cell [8]. The damper VS_x, being parallel to PE_x (and the entire length of CE_x +SE_x), generates a force proportional to the velocity of cell shortening $\dot{l}(t)$:

$$F_{VS_x} = F_{VS}(x,t) = k_{vis} \cdot \dot{l}(x,t),$$

$$k_{vis} = \beta_v \cdot e^{\alpha_v \cdot l(x,t)}, \quad (6)$$

where k_{vis} is length-dependent viscosity coefficient for VS_x[8].

The following equations define force F_x that develops by cardiomyocyte at point x:

$$F_x = F_{CE_x} + F_{PE_x} + F_{VS_x},$$

$$F_{CE_x} = F_{SE_x}, \quad (7)$$

Mechanics of the whole fiber (macrolevel)

Let $\hat{l}(x,t)$ define a deviation of cell x from its reference position in the unstretched and unexcited fiber. Therefore, the current time-dependent position of cell x at a given moment during the contractile cycle is $\hat{x} = x + \hat{l}(x,t)$.

An external serial elastic element XSE is introduced in the rheological scheme of the fiber macromodel (Fig. 2). It allows us to reproduce experiments on multicellular muscle strips and accounts for compliance in the area of the cut muscle edge, which is bound to a servomotor arm [8].

Let $l_{ex}(t)$ be a deviation of XSE length from its slack length. The force generated by XSE is defined as follows:

$$F_{XSE} = F_{XSE}(t) = \beta_3 \cdot (e^{\alpha_3 \cdot l_{ex}(t)} - 1), \quad (8)$$

where α_3 and β_3 are model parameters.

Kinematic conditions of the in-series connection between the cells in the fiber suggest that forces F_x generated by cell x are equal to each other and equal to the force of XSE:

$$F_x = F_{XSE}. \quad (9)$$

Additional conditions completing F_x determination are governed by the mode of fiber contraction. In this paper, we simulate both isometric and isotonic contractions of the fiber.

Isometric contraction is characterized by a fixed length of the fiber during the contractile cycle. Let $l_m(t)$ be a fiber deformation against its slack length. It is determined by the initial fiber prestretch by an applied preload and remains constant during the entire isometric contraction/relaxation. In the isometric mode, a displacement of the right end of the fiber during an active contraction $\hat{l}(x_F,t)$ is balanced by stretching the external passive-elastic element *XSE* so that the sum of their deformations remains constant:

$$l_m(t) = \hat{l}(x_F,t) + l_{ex}(t) \equiv \text{const}. \tag{10}$$

In the *isotonic mode* of fiber contraction, the fiber undergoes active shortening/lengthening under a fixed afterload $\overline{F} \equiv \text{const}$. In this case the fiber force, each cell force, and *XSE* force are equal to this afterload:

$$F_x = F_{XSE} = \overline{F}. \tag{11}$$

Thus, dynamics of $\hat{l}(x,t)$ and $l_{ex}(t)$ describe the macroscopic mechanics of the fiber.

Links between micro- and macromechanics

The specific feature of a continuous model of muscle mechanics is a combination of the global deformations of the fiber and the local geometry of its cells. We postulate that the local deformation of the strand at any point x in the macrospace (i.e. $\frac{\partial \hat{l}(x,t)}{\partial x}$) is equal to the relative deformation of cell x in the microspace:

$$\frac{\partial \hat{l}(x,t)}{\partial x} = l(x,t) \tag{12}$$

or the same in the integral form:

$$\hat{l}(x,t) = \int_0^x l(\xi,t)d\xi. \tag{13}$$

The above equations govern the coupling between micro- and macromechanics in the model.

Thus, during the propagation of the electrical signal from the left to the right end of the fiber, lengths of all contracting cells continuously change, providing for the global deformation of the fiber and overall force generation.

The boundary conditions (at $x = 0$ and $x = x_F$) for equation (13) during isometric contractions is given by equation (10):

$$\hat{l}(0,t) = 0, \tag{14}$$

$$\hat{l}(x_F,t) + l_{ex}(t) \equiv \hat{l}(x_F,0) + l_{ex}(0). \tag{15}$$

The initial conditions at $t = 0$ for $\hat{l}(x,0)$ and $l_{ex}(0)$ arise from the equations (7), (11) with a preload ρ applied to the fiber and prestretching it up to the value $l_m(0)$ over the slack length. Similarly, in the isotonic mode of contraction, fiber deformations $\hat{l}(x_F,\mathrm{t})$ and $l_{ex}(t)$ are determined from the equations (7), (11) for a given afterload $\overline{F}$.

Micro- and macroelectrical links

The mathematical description of the dynamics of membrane potential and ionic currents in an individual cell x is inherited from the cellular EO model [24]. Characteristics of the

depolarization and repolarization waves determine the macroscopic electrophysiology of the fiber. Let the excitation wave propagate from the left fiber end ($x = 0$) toward the right end ($x = x_F$).

Let us start with an assumption that positions of material points in the 1D fiber model do not change during the contraction-relaxation cycle. Note that such a static model is a widely used simplification in electrophysiological mathematical modeling. In this case, the electrical excitation of the fiber is governed by the cable reaction-diffusion equation [12]. The first term of the equation determines the excitation spread through diffusively coupled cells along the fiber (macrolevel), and the second term describes the change in the membrane potential $V(x, t)$ in cell x due to local transmembrane ionic currents $i_{ion}(x, t)$ (microlevel):

$$\frac{\partial V(x,t)}{\partial t} = D \cdot \frac{\partial^2 V(x,t)}{\partial x^2} - \frac{1}{C_m(x)} \cdot \sum i_{ion}(x,t), \tag{16}$$

where $C_m(x)$ denotes the membrane capacity of cell x and D is the conductivity coefficient, which determines the velocity of excitation propagation along the fiber. The coefficient D is also conventionally called a diffusion coefficient of the equation (16).

However, if the mechanical activity is taken into consideration in the fiber model, it should account for the fact that the position of cell x in the physical space is inevitably shifted from the reference slack position x due to the initial fiber prestretching and further contraction-relaxation movements. Therefore, the electrical signal propagating through cell x finds it in the other position of the macrospace.

Let cell x (material point) move to point $\hat{x} = x + \hat{l}(x,t)$ (where $\hat{l}(x,t)$ is the deviation of point x from the reference coordinate).

In this case, the diffusion term in equation (16) has to be calculated relative to point $\hat{x}$ as $D \cdot \frac{\partial^2 V(x,t)}{\partial \hat{x}^2}$ as follows:

$$\frac{\partial V}{\partial \hat{x}} = \frac{\partial V}{\partial x} \cdot \frac{\partial x}{\partial \hat{x}} = \frac{\partial V}{\partial x} \cdot \frac{1}{1 + l(x,t)}.$$

Here, we used equation (12) for the coupling between the local deformation of the fiber and relative deformation of cell x:

$$\frac{\partial \hat{x}}{\partial x} = \frac{\partial (x + \hat{l}(x,t))}{\partial x} = 1 + l(x,t),$$

$$\frac{\partial^2 V}{\partial \hat{x}^2} = \frac{(\frac{\partial V}{\partial x} \cdot \frac{1}{\partial \hat{x}})(1 + l(x,t)) - \frac{\partial V}{\partial x} \cdot \frac{\partial l(x,t)}{\partial \hat{x}}}{(1 + l(x,t))^2} = [...] =$$

$$= [...] = \frac{\frac{\partial^2 V}{\partial x^2} \cdot (1 + l(x,t)) - l_x^{'}(x,t) \cdot \frac{\partial V}{\partial x}}{(1 + l(x,t))^3}.$$

Accordingly, we come to the following modified equation:

$$\frac{\partial V}{\partial t} = D \cdot \frac{\frac{\partial^2 V}{\partial x^2} \cdot (1 + l(x,t)) - l_x^{'}(x,t) \cdot \frac{\partial V}{\partial x}}{(1 + l(x,t))^3} - \frac{1}{C_m(x)} \cdot \sum i_{ion}(x,t). \tag{17}$$

Note that the macrolevel diffusional term of equation (17) now contains the mechanical phase variable $l(x, t)$ of the cellular microlevel. Boundary conditions for the problem (17) are set as follows:

1) A short-term stimulating depolarizing current $i_{stim}(t)$ = -5 nA is aplied for 3-4 ms at the left end of the strand (at point $x = 0$), initiating excitation in the boundary cell:

$$D \cdot \frac{\partial V(0,t)}{\partial x} = i_{stim}(t).$$

Depolarization of the membrane in all other cells occurs via the electrical wave propagation from cell to cell without any additional stimulating transmembrane currents.

2) The right end of the fiber ($x = x_F$) is assumed to be electrically isolated, i.e., there are no ionic currents through the boundary point:

$$\frac{\partial V(x_F,t)}{\partial x} = 0.$$

A resting potential value is used for all fiber cells as initial conditions at $t = 0$, which is the same as in the EO model:

$$V(x,0)=V_{rest}(x).$$

Thus, the model equations define mechanisms of electro-mechanical coupling and mechano-electric feedback both at the cellular level (via mechano-dependence of Ca^{2+} kinetics, which contributes to the time course of Ca^{2+}-dependent ionic currents) and at the fiber level (via length-dependence of the diffusion component of the modified cable equation).

Several functional parameters were calculated to characterize the electrical wave. An average velocity of the depolarization wave v_{dw} along the fiber was calculated as the ratio of the initial fiber length to the propagating time Δt_{dep} from the left to the right end of the fiber. Dispersion of repolarization $DR = \Delta t_{rep}$ was calculated as the difference between the time to reach 90% of repolarization in the fiber ends. The average velocity of the repolarization wave v_{rw} was characterized by the ratio of the initial fiber length and *DR*.

Numerical methods

We used a method of splitting [6] to solve the problem (17). During each discreet time interval Δt, we at first calculated the membrane potential in each point x from the non-linear ordinary differential equation

$$\frac{dV(x,t)}{dt} = -\frac{1}{C_m(x)} \cdot \sum i_{ion}(x,t)$$

using explicit Euler or Runge-Kutta methods.

Then we used these values as initial values to solve the linear diffusion equation with corresponding boundary conditions for the same time step Δt:

$$\frac{\partial V}{\partial t} = D \cdot \frac{\frac{\partial^2 V}{\partial x^2} \cdot (1 + l(x,t)) - l_x^{'}(x,t) \cdot \frac{\partial V}{\partial x}}{(1 + l(x,t))^3}.$$

A stable implicit difference scheme was built to solve the problem. The equations were discretized with a time step of $\Delta t = 10^{-5}$ s and a spacial step of $\Delta x = 0.25$ mm. This gives a system of linear algebraic equations with a tridiagonal matrix for numerical values V_j^i for action potential $V(x, t)$ at point x_i at time t_j. The linear system was solved by a tridiagonal matrix algorithm.

The mechanical block of the model was solved in the same discretization nodes. Macrovariables $\hat{l}(x_i, t_j)$ and $l_{ex}(t_j)$ were calculated by numerical solution of equations (7), (9) in parallel with numerical integration of (13) with consistent boundary conditions (10) or

(11). Cellular mechanics was calculated together with ionic concentrations and membrane potential at each discreet point x_i by numerical integration of the corresponding cellular EO model.

ELECTRO-MECHANICAL COUPLING IN 1D CARDIAC FIBER

Here, we demonstrate the effects of the electrical and mechanical asynchrony arising in a 1D homogeneous fiber model of 40 mm initial slack length from the interference between the electrical and mechanical waves excited at 1 Hz.

In the homogeneous fiber, an electrical asynchrony (the time difference in regional excitation timing) is determined by the velocity of excitation wave propagation along the fiber. The mechanical asynchrony in the fiber is induced by the electrical asynchrony, since the deformation field depends on the level of mechanical activation of each cell at any moment of the electrical wave propagation and relaxation.

Model configurations

In this paper, we started with the full fiber model where all the cross-links between the macro- and micromechano-electric interactions are accounted for. Then we excluded either electrical or mechanical coupling between the cells in the tissue and analyzed a separate contribution of the links in the overall system performance. Namely, the following 4 types of 1D model modifications were considered:

EMM (Electro-Mechanical Model) is the complete model of the electrical and mechanical coupling between the cells in the fiber, as described above. Dynamic change in cell lengths is taken into consideration when an excitation wave propagates along the fiber (see equation (17))

MM (Mechanical Model) is the *EMM* with eliminated electrical (diffusional) coupling between the cells. Thus, only mechanical interactions are taken into account on the macrolevel while the activation sequence is simulated by applying fixed delays between cell excitation along the fiber. The delays between adjacent fiber segments are calculated from the overall v_{dw} obtained in the *EMM*. Both the mechanical asynchrony and microlevel electro-mechanical coupling contribute to the *MM* behavior.

EM (Electrical Model) is the model of the fiber electrical activity with only electrical coupling between the cells. Mechanical interactions between cells are excluded from the *EMM* by fixing initial cell positions during excitation wave propagation. Cellular mechanical activity is predetermined in the model as that calculated in isolated cells.

Model *RM* is the reference model of the fiber. It simulates purely homogeneous fiber with simultaneous excitation of identical cells. Contracting cells of this fiber behave like isolated cardiomyocytes, isopotentially, and isomechanically. Electrical and mechanical asynchrony is excluded, and any factors of cellular interaction are totally eliminated in the *RM* model.

Steady-state values of phase variables in the *RM* model at pacing interval of $T = 1$ s were taken as the initial values in *MM*, *EM*, and *EMM*, which then approached their own steady states.

Electro-mechanical activity in 1D fiber models in isometric contractions

Electrical activity in the EMM in isometric contractions

In simulations presented below, we used the *EMM* with various diffusion coefficients D to simulate effects of the velocity of the depolarization wave on fiber performance. Before excitation the fiber was prestretched 25% to the initial length of $L_{init} = 50.5$ mm with a corresponding sarcomere length of 2.1μm and then stimulated at the left end of the fiber. After 10 beats the model almost reached steady-state contractions, which are used in the figures below.

Figure 3,**A** shows dependence of the average velocities of depolarization (v_{dw}, *diamonds*) and repolarization (v_{rw}, *crosses*) waves on the diffusion coefficient D (D = 50, 75, 100, 150, 300, 400 mm^2/s). Obviously, the higher the diffusion coefficient, the faster depolarization spreads along the fiber, but this dependence is not linear. The velocity of depolarization at the smallest D = 50 mm^2/s is 0.2 mm/ms, then grows to 0.4 mm/ms when D is doubled, and to 0.9 mm/ms when D = 400 mm^2/s (D increased by a factor of 8).

It is known that the speed of propagation of the electrical excitation wave in the myocardial tissue is normally 0.3-0.5 m/s. This range of velocities in our model corresponds to the range of the diffusion coefficient D = 100-300 mm^2/s. Deviations from these values may occur in pathology. For example, in patients with congenital and acquired heart diseases, as well as during hypoxia, the conduction of excitation may slow down.

The dependence for the velocity of repolarization is ascending too, but it is steeper than that for v_{dw}.

In the framework of the model, we found that the average velocity of the depolarization wave is always less than the average velocity of the repolarization wave. The minimum difference between the velocities is seen at the smallest coefficient D. An increase in D draws them apart from each other.

As can be derived from (Fig. 3,**C**), in the homogeneous fiber both waves spread in the same direction from left to right. This is not consistent with experimental data [26] showing that depolarization and repolarization waves are directed oppositely. As we have shown earlier in our discrete models [23], transmural heterogeneity of the electrical and mechanical properties of cardiomyocytes and the activation sequence directed from the slow- to fast-contracting elements of in-series muscle chain are the key conditions for the opposite direction of the repolarization wave against depolarization.

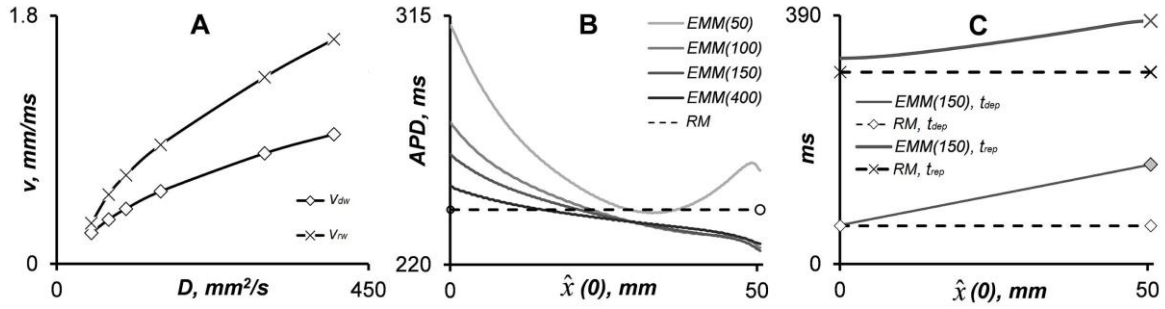

Fig. 3. Parameters of the electrical waves in the 1D fiber model. **A.** Dependence of the velocities of depolarization (v_{dw}) and repolarization (v_{rw}) waves on the diffusion coefficient D in the *EMM*. **B.** Distribution of action potential duration along the fiber in the *EMM* at different diffusion coefficients (solid lines, D = 50, 100, 150, 400 mm^2/s) against that in the *RM* (dotted line). **C.** Distribution of the depolarization onset (t_{dep}) and the end of repolarization (t_{rep}) along the fiber in the *EMM* at D = 150 mm^2/s (solid lines) *vs* the *RM* model (dotted lines). Spatial coordinate $\hat{x}(0)$ on the horizontal axis in panels **B** and **C** shows the initial cell position in the fiber.

Correlations between the time characteristics of depolarization and repolarization waves are also shown in Figure 4,**A**, where dispersion of repolarization (*DR*) is plotted against the time delay between the onset of excitation in the right and left ends of the fiber (Δt_{dep}) at different diffusion coefficients D. Obviously, the smallest Δt_{dep} corresponds to the greatest diffusion coefficient D that we used. The dotted line on the plot demonstrates a reference line $DR = \Delta t_{dep}$, which would occur if *APD*s of the cells were not affected by cell coupling. As is shown in Figure 4,**A**, the dependence for the *EMM* lies under this reference line. This is a result of the changes in *APD* of cardiomyocytes along the fiber due to their interactions within the *EMM* (see Fig. 3,**B**).

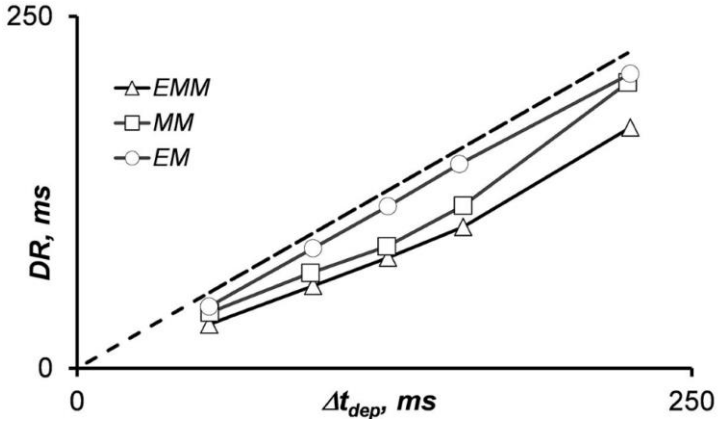

Fig. 4. Dependence of *DR* on the time delay between the excitation onset in the border cells of the fiber (Δt_{dep}) in the complete *EMM* and in reduced *EM* and *MM* at different diffusion coefficients *D*. Contrast the dependencies with a reference dotted line $DR = \Delta t_{dep}$.

Figure 3,**B** demonstrates the gradients in *APD*(*x*) developed in cardiomyocytes along the fiber models. The data are shown for different diffusion coefficients in the *EMM*. The dotted line shows the control *APD* in cardiomyocytes of the *RM* (*APD* = 241 ms). For all diffusion coefficients, an electrical asynchrony of cell activation in the fiber results in *APD* lengthening in cells located closer to the left border as compared to the control *APD* in the *RM*. We observed a gradual *APD*(*x*) shortening along the fiber down to the values less than the control *APD* at the right fiber end at the diffusion coefficient greater than $D = 50$ mm^2/s. At this slow propagation velocity, *APD* change was not monotonous. The heterogeneity in *APD* increased with a decrease in the diffusion coefficient. So, in the left border cell, *APD* increased from 250 ms at $D = 400$ mm^2/s up to 311 ms (30%) at $D = 50$ mm^2/s, while *APD*s at the right fiber end were similar at medium and high *D* values.

The Figure 3,**B** reveals that for small values of the diffusion coefficient ($D = 50$ mm^2/s) *APD* in the cells located in the right third of the fiber is the greater the closer is the point (cell) to the right edge (except the rightmost points). This occurs due to the fact that at the time, when the excitation wave comes to the right segment, the cells at the left edge, which were stimulated first, have already completed their contraction and do not oppose to the shortening of the right cells.

Therefore both amplitudes and the velocities of the right cells shortening increase comparing to the cases of a higher diffusion coefficient (Fig. 5,**D** vs. 5,**C**). The greater velocities and the peak shortenings of the sarcomeres in these cells lead to their calcium inactivation (see section Mechanics of the cellular level (microlevel)) for the low values of the diffusion coefficient as compared to the higher values. In other words, dissociation of CaTnC complexes increases resulting in an increase in the concentration of free intracellular Ca^{2+} and thus in an increase in *APD* in these cells at small values of the diffusion coefficient. A sharp drop of *APD* in the rightmost cells observed in Figure 3,**B** is a consequence of the particular boundary condition used in the presented numerical experiment (see section Micro- and macroelectrical links).

The difference in *APD* between the border cells (ΔAPD) in the *EMM* at different diffusion coefficients is plotted against the depolarization delay Δt_{dep} (see Fig. 3,**B**, *triangles*). The slower depolarization wave (i.e., increase in Δt_{dep}) makes the fiber more electrically heterogeneous.

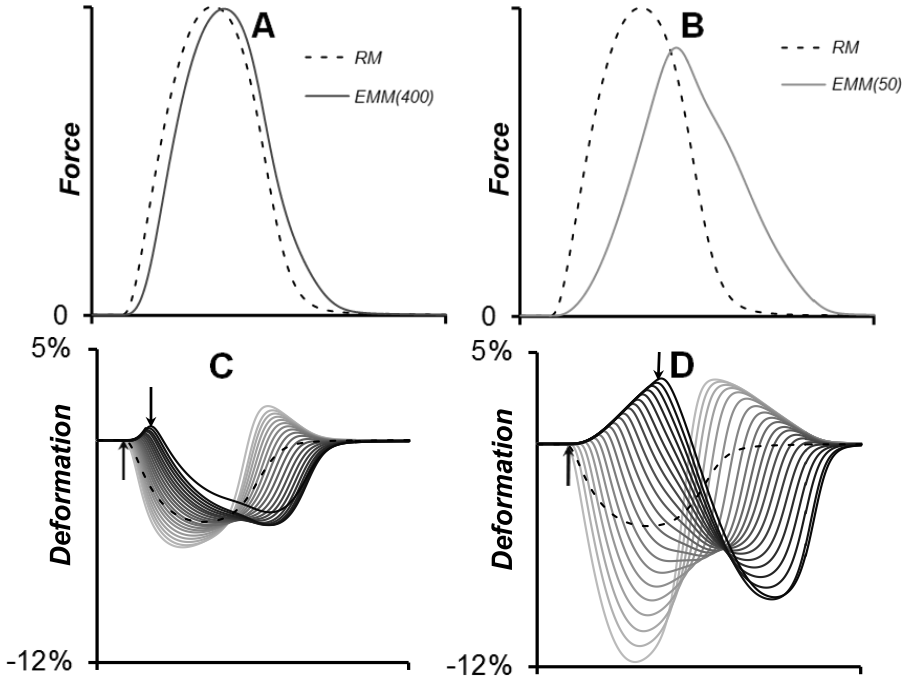

Рис. 5. Mechanical activity in the *EMM* at various diffusion coefficients: **A, B.** Force generated by the *EMM* (solid lines) in the case of D = 400 mm^2/s (panel **A**) and D = 50 mm^2/s (panel **B**) against the isometric contraction of the *RM* (dashed line). Force is normalized to the peak force in the *RM*; **C, D.** Time course of cell deformations (expressed as % of initial cell length) along the fiber at high (**C**, D = 400 mm^2/s) and low (**D**, D = 50 mm^2/s) conduction velocity. Excitation onsets in the border cells are shown by up and down arrows, respectively. Dashed line shows cell deformation in the *RM*.

Mechanical activity in the EMM during isometric contractions

The model of fiber electro-mechanics allowed us to analyze how changes in the electrical activity of coupled cardiomyocytes in the full *EMM* are related to the mechanical activity of the cells.

Figure 5 demonstrates the changes in the mechanical activity of the whole fiber and its interacting cardiomyocytes in isometric contractions of the *EMM* against the control behavior in the *RM*. When a depolarization wave spreads along the fiber, *APD* generation in the excited cells is followed by their contraction and force is developed by the fiber. In the *RM*, all the cells are excited and activated simultaneously. Therefore, they shorten equally (see dotted lines in Fig. 5) and collectively pull the common extra-series elastic element *XSE* (see Fig. 1) generating fiber force. When cells inactivate and cannot resist *XSE*, they are stretched back and fiber force falls (Fig. 5). In the *EMM* fiber, there is a time sequence of cardiomyocytes excitation and mechanical activation along the fiber with significant time delays between distant regions. Due to the much slower electrical wave propagation as compared with almost instantaneous propagation of the mechanical signals, all fiber cells instantaneously respond to a change in the mechanical activity in any excited region. Cells activated earlier begin shortening and stretch the later-activated passive cells before the excitation wave approaches them (see solid lines in Fig. 5). When activation captures the whole fiber, all cardiomyocytes may collectively shorten, so force generated by the fiber increases. Then, earlier activated cardiomyocytes weaken and are stretched by the later-activated cardiomyocytes, and fiber force goes down. So we can see that an electrical excitation wave in a morphologically homogeneous fiber not only causes heterogeneity in the electrical activity of coupled cardiomyocytes but also gives rise to a significant mechanical heterogeneity.

Figure 5 demonstrates cell cyclic deformations and force development in the *EMM* fiber at various velocities of excitation propagation D = 400 mm^2/s and D = 50 mm^2/s. A decrease in the excitation spread increased the time delay between excitation of fiber border cells from

54 ms to 225 ms. This results in a significant increase in the mechanical heterogeneity between cardiomyocytes along the fiber. Cardiomyocytes from the left part of the fiber activated earlier underwent much greater shortening and stretched the later-activated cardiomyocytes at the right part to a greater extent (1% at D = 400 mm^2/s and 4% at D = 50 mm^2/s). Note that amplitudes of cardiomyocyte shortening in all the fiber regions were greater than those in the reference model where cardiomyocytes contract simultaneously, e.g., the slow excitation propagation causes about a 3 times increase in the maximal cell shortening amplitude against the control. At rather high velocities of fiber excitation, force development was not significantly affected by cardiomyocyte interactions as compared to the control isopotential fiber (Fig. 5,**C**). In contrast, slowing down excitation and the following increase in the strain heterogeneity along the fiber causes a significant decrease in force production and a decrease in the velocity of force development and relaxation during fiber isometric twitch. In the *EMM* at D = 50mm^2/s, the peak force decreased 13%, the time to peak force increased to 294 ms *vs* 215 ms, and the characteristic time to 70% relaxation increased to 210 ms *vs* 143 ms compared to the *RM*.

Role of electrical and mechanical coupling in fiber performance

The results we presented above were obtained in the full *EMM* where both electrical and mechanical couplings between cells in the fiber were taken into account. To assess the role of each coupling separately, we contrasted results of simulations obtained in the *EMM* with that of reduced *EM* and *MM* (see section Model configurations, Fig. 4).

In the *EM*, fiber cells communicate electrically only. In this case *APD* monotonously decreases along the fiber according to the depolarization wave front, which gives negative values of Δ*APD* shown in Figure 4,**B**. This decrease is ensured from the electrotonic interactions between the cells. It is seen that the electrical coupling did not affect *APD* as much as it occurs in the *EMM*, even at decreasing velocity of the excitation spread. The difference in *APD* in border cells, Δ*APD*, varies from -9.5 ms to -11.4 ms with increasing Δt_{dep} in the *EM*. Similarly, dependence of the dispersion of repolarization *DR* on Δt_{dep} lies slightly below and almost parallel to the reference line $DR = \Delta t_{dep}$ (Fig. 4,**A**).

In the *MM*, cells are coupled mechanically while electrotonic interaction is excluded. Cells in the *MM* are stimulated with the same timing as in the *EMM*, but the electrical signal does not propagate from cell to cell. In this case the changes in the cell electrical activity and the mechanical deformations in the *MM* are qualitatively similar to those registered in the *EMM*. As shown in Figure 4, dependencies of *APD* and *DR* on excitation velocity have similar characters, but the quantitative effects of cellular coupling on *APD* in the *EMM* occur more expressed due to combined electro-mechanical interactions. As a result, *DR* in the *EMM* occurs even less than in the *MM*. Comparison of the models suggest that the dynamic deformations arising from the mechanical interactions between coupled cardiomyocytes play a key role in adjusting the mechanical activity of the fiber and also, via intracellular mechano-electric feedback mechanisms, they significantly affect electrical properties of cells in cardiac tissue.

Afterloaded contractions in the 1D fiber model

The isometric contractions we demonstrated above are widely used in experimental cardiac physiology to mimic isovolumetric contraction of the intact ventricle in isolated myocardium preparations (trabeculae or papillary muscles). However, the isovolumetric mode takes place during only short phases of the entire cycle of ventriclular contraction and relaxation. The ejection phase under some afterload is the most important part of ventricular contraction determining overall heart pump function. During this phase collective shortening/lengthening of the ventricular myocardial fibers occurs, which results in volume change.

The afterloaded mode of contractions is widely used in experiments on isolated cardiac samples to study load-dependence of cardiac mechanical function. Here, a constant afterload is applied on the muscle, which can cyclically shorten and lengthen under this load when excited. Before the shortening phase, the fiber develops isometric force until it reaches the afterload level. Then the fiber is allowed to shorten (isotonic contraction) and to lengthen back (isotonic relaxation) under the fixed load $\overline{F}$. When the muscle length approaches its initial value, the length is fixed again, and muscle finally relaxes isometrically. The initial muscle length is called end-diastolic length, and the minimal length approached during contraction is often called end-systolic length in the afterloaded twitch.

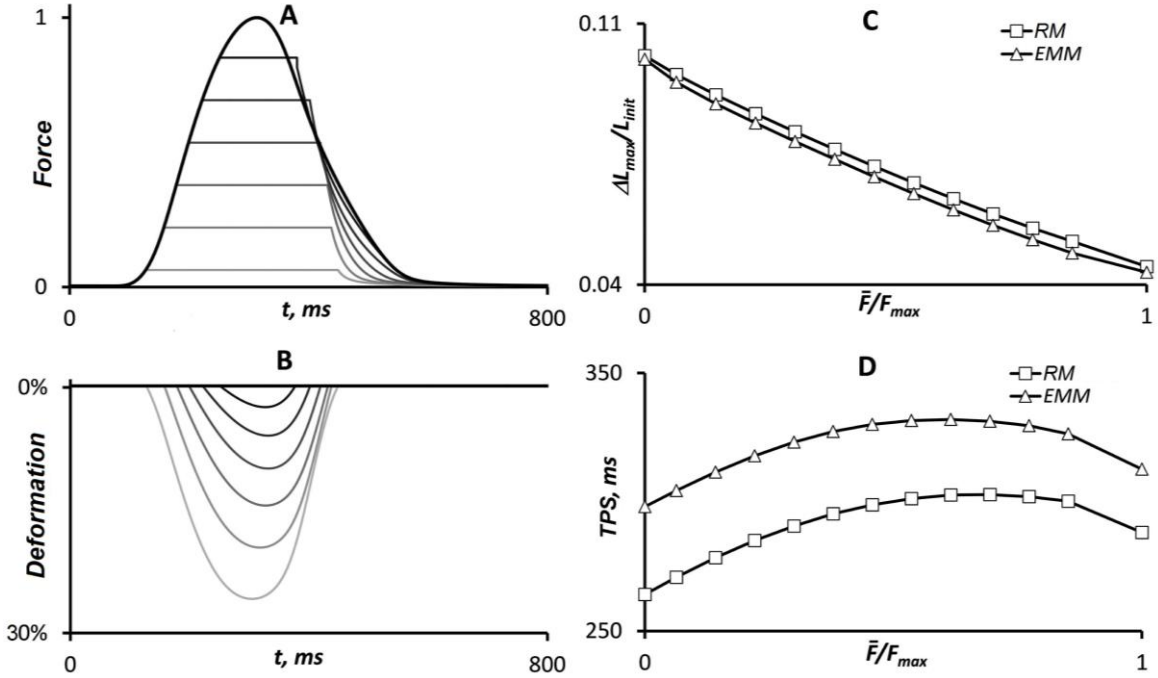

Fig. 6. Isometric (bold black lines) and afterloaded twitches (gray lines) of a fiber under different loads $\overline{F}$ simulated in the *EMM*. **A, B.** Force generated by the fiber (normalized by the peak isometric force F_{max}) at an initial fiber length L_{init} = 50.5 mm and D = 300 mm^2/s is shown against corresponding fiber shortening (expressed as % of L_{init}). **C.** Dependence of the end-systolic shortening (ΔL_{max}) on afterload in the *EMM* is compared with that of the *RM*. **D.** Dependencies of the time to peak shortening (*TPS*) on afterload in the *EMM* and *RM* are shown.

Figure 6 demonstrates isometric and afterloaded twitches simulated in the *EMM* at different afterloads $\overline{F}$. The lower that $\overline{F}$ is, the earlier that isotonic shortening begins (Fig. 6,**B**). In accordance with experimental data, a decrease in load results in an increase in end-systolic shortening of the fiber (Fig. 6,**C**) and an increase in the velocity of shortening (the latter can be derived from Fig. 6,**C**, **D**) [24]. A comparison with the respective data obtained in the isopotential *RM* shows that the electrical and mechanical asynchrony in the *EMM* affect parameters of muscle contraction, especially increasing time to peak shortening (Fig. 6,**D**).

We considered in the 1D model an important phenomenon of load dependence of the relaxation characteristic to normal myocardium (Fig. 6,**A**, **B**) [3]. This effect was earlier validated in our cellular model [5, 7] incorporated now in the fiber model. The fiber model also proved to simulate this phenomenon correctly:

1. The duration of the isotonic phase of contraction became shorter with load decrease (Fig. 6,**A**);

2. The lower afterload resulted in a higher velocity of fiber lengthening during isotonic relaxation (Fig. 6,**B**).

Not only the mechanical but also the electrical parameters of fiber activity depend on the applied load. In accordance with experimental data obtained in ferret [16] and cat [11], the *EMM* produces an increase in cell *APD* with a decrease in afterload (Fig. 7,**A**). Earlier we simulated this effect in the EO model and identified mechanisms of cellular mechano-electric coupling responsible for this effect [24]. Similar qualitative dependencies of *APD* on mechanical load were obtained in all cells in the *EMM*. An increase in cellular *APD* with a decrease in load is correlated with an increase in cellular shortening during afterloaded contraction in the fiber (Fig. 7,**B**). Moreover, we found that a quantitative *APD* increment depended on the cell position within the fiber (Fig. 7,**A**). Surprisingly, the greater change in *APD* was observed in the later-activated cardiomyocytes in the fiber, so the *APD* distribution along the fiber became more homogeneous during low-loaded contractions as compared to heavy-loaded isometric twitch (Fig. 7,**A**).

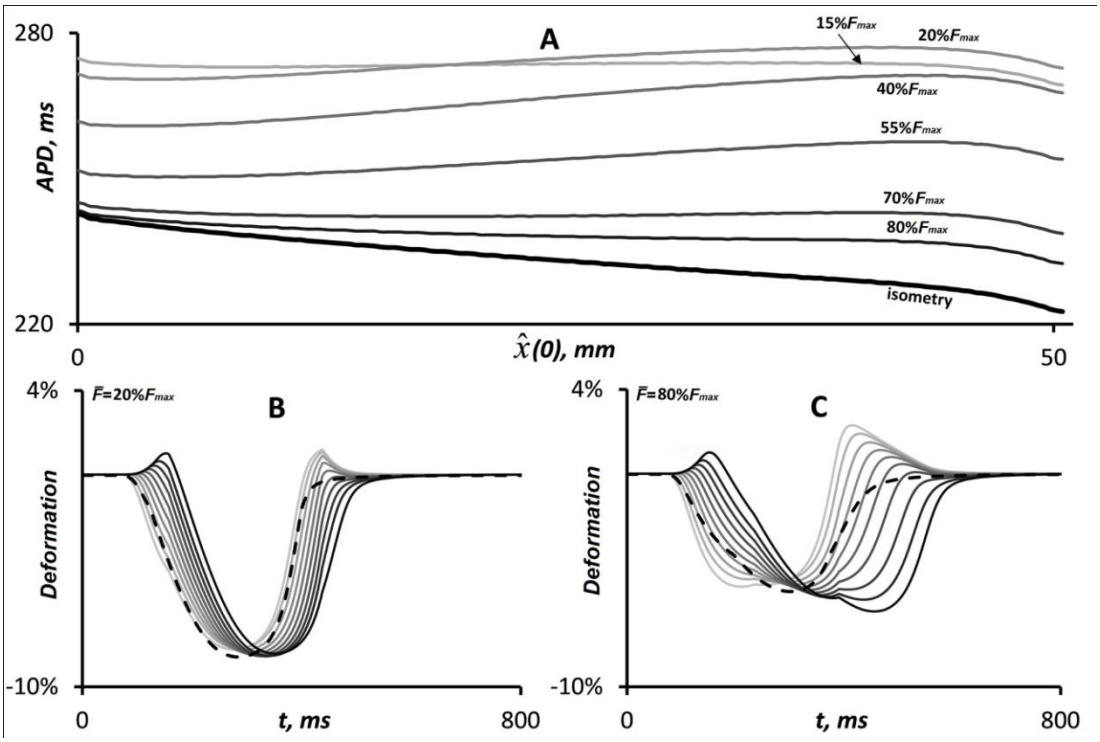

Fig. 7. Effects of the load on cell *APD* and deformation pattern during fiber afterloaded contractions in the *EMM*. **A.** Gradients of action potential duration along the fiber during isometric (black thick line) and afterloaded (gray gradient lines) twitches under different loads $\bar{F}$. **B, C.** Cell deformations (gray lines) during afterloaded twitches under $\bar{F}$ = 20% of F_{max} (**B**) and $\bar{F}$ = 80% of F_{max} (**C**). The dotted line shows cell deformation in the *RM* under the same afterloads.

This effect can be explained within the framework of the model. The lower the applied load, the shorter is the isometric phase of afterloaded contraction where cardiomyocytes actually interact and influence each other, thus their electro-mechanical behavior becomes more uniform (Fig. 7). Note that the later-activated cardiomyocytes are prestretched during the isometric phase of afterloaded contraction (Fig. 7,**B**). At higher afterloads this phase is longer, and a higher prestretch together with less shortening favors a greater *APD* shortening in later-activated cardiomyocytes as compared with those activated earlier.

DISCUSSION AND CONCLUSIONS

Mathematical models are widely used in cardiac physiology. We have earlier developed mathematical model of the electromechanical coupling (EMC) in the single cardiomyocytes [23, 24]. Here we suggest a model of the heart muscle multicellular fiber, describing both electrical excitation propagation and the fiber's contraction. At the cellular level this fiber model co-opts the above model of the intra-cardiomyocyte EMC.

1D modeling of electrical and mechanical functions of the myocardial tissue is an important step in the course of the development of 3D electromechanics models. There are a number of principal problems that may be solved only by means of 3D models. For instance, only 3D or at least 2D modeling makes it possible to formulate and analyze one of the important tasks of the electrophysiology of the heart: assessment of the role of electrical anisotropy of cardiac tissue (i.e. the ratio of the conductivity coefficients along and across the myocardial fibers) in cardiac performance. Experimental data show that the ratio of longitudinal to transverse conduction velocities ranges between 3 [19] and 2.1 [14]. Of course, the effects of anisotropy can be studied only on models which dimension is higher than 1. In particular, we participate in such study involving a 3D model [20]. Furthermore, complex fiber twist in the heart ventricle wall is an important factor contributing to the mechanical function. This feature can also be displayed only in three-dimensional models.

Nevertheless, multicellular fiber is a key participant of the heart performance, and therefore it seems to be reasonable to consider 1D models as minimal models of the cardiac tissue. Indeed, electrical wave activating cardiomyocytes does propagate faster along the fiber as compared to the transverse direction. Moreover, both mechanical tension developed by the activated cardiomyocytes and their corresponding deformations are directed along the fiber determining principally the total mechanical activity of the ventricle. These processes can be investigated in detail in the framework of one-dimensional models. Moreover, being less complicated, than 3D and 2D models, one-dimensional models are more relevant tools for the analysis of cross-links within the EMC of cardiac fiber and its constituent cells. Such an analysis has been fulfilled in part within our work.

Due to the incorporation of the cellular model into the fiber one we ensured for the integration of cardiac excitation-contraction coupling and mechano-electric feedback mechanisms at both the cellular and tissue level. As 1D fiber model is intented to predict new loops of the EMC arising on the multicellular level, it is very important that incorpareted cellular model has been earlier carefully validated by comparison with experimental data [5, 7, 17].

We have shown that the electrical and mechanical activation sequence, which is intrinsic to myocardium contraction in intact heart, gives rise to the functional nonuniformity of the electrical and mechanical properties of coupled cardiomyocytes and affects overall function of the tissue. These model predictions are consistent with experimental data showing significant heterogeneity in the electrical characteristics and in the dynamic shortening of different ventricular regions in intact ventricle [1, 21].

The model predicts that slowing down excitation spread along the fiber during isometric twitches causes an increase in cellular functional heterogeneity, a decrease in the velocity of the repolarization wave, and an increase in dispersion of repolarization producing a substrate of arrhythmia. Moreover, an increase in the time delays of regional mechanical activation in the fiber increases local cell deformations and has a negative effect on fiber contractility slowing down both contraction and relaxation and decreasing maximal force production.

In the afterloaded mode of contractions, we showed that an increase in the mechanical load may result in an increase in the electrical gradients in the tissue, which is also known as an arrhythmogenic factor. This result has clear clinical translation showing possible tuning of the cardiomyocytes due to high blood pressure. The results we obtained in afterloaded contractions clearly show the significance of the isometric entrant phase of cardiac

contraction, which appears to not be static but a highly dynamic phase predetermining further fiber isotonic shortening and relaxation. These results are consistent with experimental data registered for the intact heart and showing significant dynamic reconfigurations of transmural and longitudinal ventricular regions during the isovolumetric phase of contraction, which contribute to effective ventricular ejection [2].

By eliminating either electrical or mechanical cellular interactions within the reduced fiber models, we have shown that both circuits of cell coupling are significant and collectively evolve fiber functional heterogeneity. At the same time, we showed that mechanical coupling and cellular mechano-electric feedback are stronger contributors to this modulation of cellular functions.

Model analysis allows us to reveal the cellular mechanisms underlying the macroscopic effects of electro-mechanical coupling in myocardium. Mechanical interactions of the asynchronously activated cells evolve dynamic strain fields in the tissue. This via cooperativity mechanisms affects mechano-dependent calcium activation of myofilaments in the cells, and therefore influences intracellular calcium kinetics and AP generation. Therefore, mechanical wave affects the electrical wave of repolarization and dispersion of repolarization in the fiber.

Considering in this paper the model of initially homogeneous fiber generating nonuniformity due to its functioning gives the only first step in understanding the role of inherent heterogeneity in individual electro-mechanical properties of cardiomyocytes in different ventricular regions intrinsic to the intact heart. This problem has been earlier addressed with the help of simplified tissue models and has been discussed in several of our papers [23, 24]. This 1D continuous model we developed gives us a more consistent tool to study further consequences of electro-mechanical coupling in the heterogeneous myocardium.

In our study we try to stratify important pathways of the fiber contraction regulation various mechano-electric feedbacks including (e.g., intracellular and intercellular ones). We introduce them into the model not simultaneously but step-by-step to assess individual contribution of each one to the total electrical and mechanical function of the virtual fiber (see section Model configurations). We have not accounted for in the model some more MEFs. Two of them are worth special mentioning.

(i) On the intracellular level, there is a feedback provided with stretch-activated ionic channels.

(ii) On the tissue level, there is a length-dependence of the cell conductivity (a length-dependence of the diffusion coefficient D), which should account for dynamic change in the cross-section of cells at their constant volume.

We are going to introduce (i) and (ii) in the fiber model later on and find out how these MEFs may contribute to the electrical and mechanical performance of the heart muscle fiber.

Development of the program code for 1D model of myocardium is supported by Programe of the Presidium of the Russian Academy of Sciences (II.4П), mathematical modeling of cooperative mechanisms underlying MEF in cardiomyocytes is supported by the RFBR (#13-04-00365) and by the RAS Program (#15-5-4-8), analysis of intracellular mechanisms underlying long-term effects of cell coupling in the tissue is supported by the RBRF (#14-01-00885) and effects of electro-mechanical coupling in myocardial tissue is supported by The Russian Science Foundation (#14-35-00005).

REFERENCES

1. Ashikaga H., Coppola B.A., Hopenfeld B., Leifer E.S., McVeigh E.R., Omens J.H. Transmural dispersion of myofiber mechanics: implications for electrical heterogeneity in vivo. *J. Am. Coll. Cardiol*. 2007. V. 49. № 8. P. 909–916.
2. Ashikaga H., van der Spoel T.I., Coppola B.A., Omens J.H. Transmural myocardial mechanics during isovolumic contraction. *JACC Cardiovasc. Imaging*. 2009. V. 2. № 2. P. 202–211.

3. Brutsaert D.L. Nonuniformity: a physiologic modulator of contraction and relaxation of the normal heart. *J. Am. Coll. Cardiol*. 1987. V. 9. № 2. P. 341–348.
4. Clayton R.H., Bernus O., Cherry E.M., Dierckx H., Fenton F.H., Mirabella L., Panfilov A.V., Sachse F.B., Seemann G., Zhang H. Models of cardiac tissue electrophysiology: progress, challenges and open questions. *Prog. Biophys. Mol. Biol*. 2011. V. 104. № 1–3. P. 22–48.
5. Izakov V., Katsnelson L.B., Blyakhman F.A., Markhasin V.S., Shklyar T.F. Cooperative effects due to calcium binding by troponin and their consequences for contraction and relaxation of cardiac muscle under various conditions of mechanical loading. *Circ. Res*. 1991. V. 69. № 5. P. 1171–1184.
6. Jahnke T., Lubich C. Error bounds for exponential operator splittings. *BIT Numerical Mathematics*. 2000. V. 40. № 4. P. 735–744.
7. Katsnelson L.B., Nikitina L.V., Chemla D., Solovyova O., Coirault C., Lecarpentier Y., Markhasin V.S. Influence of viscosity on myocardium mechanical activity: A mathematical model. *Journal of Theoretical Biology*. 2004. V. 3. № 230. P. 385–405.
8. Katsnelson L.B., Sulman T., Solovyova O., Markhasin V.S. Role of myocardial viscoelasticity in disturbances of electrical and mechanical activity in calcium overloaded cardiomyocytes: mathematical modeling. *J. Theor. Biol*. 2011. V. 272. № 1. P. 83–95.
9. Katsnelson L.B., Sulman T.B., Solovyova O.E., Markhasin V.S. Cooperative mechanisms of thin filament activation and their contribution to the myocardial contractile function. Assessment in a mathematical model. *Biophysics*. 2009. V. 54. № 1. P. 39–46.
10. Katsnelson L.B., Vikulova N.A., Kursanov A.G., Solovyova O.E., Markhasin V.S. Electro-mechanical coupling in a one-dimensional model of heart muscle fiber. *RJNAMM*. 2014. V. 29. № 5. P. 275–284.
11. Kaufmann R.L., Lab M.J., Hennekes R., Krause H. Feedback interaction of mechanical and electrical events in the isolated mammalian ventricular myocardium (cat papillary muscle). *Pflugers Arch.* 1971. V. 324. № 2. P. 100–123.
12. Keener J.P., Sneyd J. *Mathematical Physiology: I: Cellular Physiology*. Springer, 2008.
13. Kerckhoffs R.C.P., Healy S.N., Usyk T.P., McCulloch A.D. Computational methods for cardiac electromechanics. *Proceedings of the IEEE*. 2006. V. 94. № 4. P. 769–782.
14. Kleber A.G., Rudy Y. Basic mechanisms of cardiac impulse propagation and associated arrhythmias. *Physiol. Rev*. 2004. V. 84. P. 431–488.
15. Kohl P., Sachs F., Franz M.R. *Cardiac mechano-electric coupling and arrhythmias.* OUP Oxford, 2011. 512 p.
16. Lab M.J., Allen D.G., Orchard C.H. The effects of shortening on myoplasmic calcium concentration and on the action potential in mammalian ventricular muscle. *Circ. Res.* 1984. V. 55. № 6. P. 825–829.
17. Markhasin V.S., Balakin A.A., Katsnelson L.B., Konovalov P., Lookin O.N., Protsenko Y., Solovyova O. Slow force response and auto-regulation of contractility in heterogeneous myocardium. *Prog. Biophys. Mol. Biol*. 2012. V. 110. № 2–3. P. 305–318.
18. Noble D., Varghese A., Kohl P., Noble P. Improved guinea-pig ventricular cell model incorporating a diadic space, I_{Kr} and I_{Ks}, and length- and tension-dependent processes. *Can. J. Cardiol*. 1998. V. 14. № 1. P. 123–134.
19. SaffitzJ.E., KanterH.L., GreenK.G., TolleyT.K., BeyerE.C Tissue-specific determinants of anisotropic conduction velocity in canine atrial and ventricular myocardium. *Circ. Res*. 1994. V. 74. P. 1065–1070.
20. Pravdin S.F., Dierckx H., Katsnelson L.B., Solovyova O., Markhasin V.S., Panfilov A.V. Electrical Wave Propagation in an Anisotropic Model of the Left

Ventricle Based on Analytical Description of Cardiac Architecture. *PLoS ONE*. 2014. V. 9. № 5.

21. Sengupta P.P., Khandheria B.K., Korinek J., Wang J., Jahangir A., Seward J.B., Belohlavek M. Apex-to-base dispersion in regional timing of left ventricular shortening and lengthening. *J. Am. Coll. Cardiol*. 2006. V.47. № 1. P. 163–172.
22. Shaw R.M., Rudy Y. Ionic mechanisms of propagation in cardiac tissue. Roles of the sodium and L-type calcium currents during reduced excitability and decreased gap junction coupling. *Circ. Res*. 1997. V. 81. № 5. P. 727–41.
23. Solovyova O., Katsnelson L.B., Konovalov P., Lookin O., Moskvin A.S., ProtsenkoY.L., Vikulova N., Kohl P., Markhasin V.S. Activation sequence as a key factor in spatio-temporal optimization of myocardial function. *Philos. Trans. R. Soc. Lond. Ser. A Math. Phys. Eng. Sci.* 2006. V. 364. № 1843. P. 1367–1383.
24. Solovyova O., Vikulova N., Katsnelson L.B., Markhasin V.S., Noble P.J., Garny A., Kohl P., Noble D. Mechanical interaction of heterogeneous cardiac muscle segments in silico: effects on Ca^{2+} handling and action potential. *IJBC*. 2003. V. 13. № 12. P. 3757–3782.
25. Trayanova N.A. Whole-heart modeling: applications to cardiac electrophysiology and electromechanics. *Circ. Res*. 2011. V. 108. № 1. P. 113–128.
26. Wan X., Bryant S.M., Hart G. A topographical study of mechanical and electrical properties of single myocytes isolated from normal guinea-pig ventricular muscle. *J. Anat.* 2003. 202. № 6. P. 525–536.

Received October 07, 2015.
Published November 16, 2015.